Stretching DNA with Optical Tweezers

Michelle D. Wang,* Hong Yin,# Robert Landick,§ Jeff Gelles,# and Steven M. Block*
*Department of Molecular Biology, Princeton University, Princeton, New Jersey 08544; #Department of Biochemistry, Brandeis University, Waltham, Massachusetts 02254; and §Department of Bacteriology, University of Wisconsin, Madison, Wisconsin 53706 USA

ABSTRACT Force-extension (*F-x*) relationships were measured for single molecules of DNA under a variety of buffer conditions, using an optical trapping interferometer modified to incorporate feedback control. One end of a single DNA molecule was fixed to a coverglass surface by means of a stalled RNA polymerase complex. The other end was linked to a microscopic bead, which was captured and held in an optical trap. The DNA was subsequently stretched by moving the coverglass with respect to the trap using a piezo-driven stage, while the position of the bead was recorded at nanometer-scale resolution. An electronic feedback circuit was activated to prevent bead movement beyond a preset clamping point by modulating the light intensity, altering the trap stiffness dynamically. This arrangement permits rapid determination of the *F-x* relationship for individual DNA molecules as short as ~1 μm with unprecedented accuracy, subjected to both low (~0.1 pN) and high (~50 pN) loads: complete data sets are acquired in under a minute. Experimental *F-x* relationships were fit over much of their range by entropic elasticity theories based on worm-like chain models. Fits yielded a persistence length, L_P, of ~47 nm in a buffer containing 10 mM Na^+. Multivalent cations, such as Mg^{2+} or spermidine^{3+}, reduced L_P to ~40 nm. Although multivalent ions shield most of the negative charges on the DNA backbone, they did not further reduce L_P significantly, suggesting that the intrinsic persistence length remains close to 40 nm. An elasticity theory incorporating both enthalpic and entropic contributions to stiffness fit the experimental results extremely well throughout the full range of extensions and returned an elastic modulus of ~1100 pN.

INTRODUCTION

The mechanical flexibility of DNA plays a key role in all of its cellular functions, including folding, packaging, regulation, recombination, replication, and transcription. The intimate connections between DNA's molecular interactions and its physical properties are therefore of considerable interest to biologists (Yang et al., 1995). Moreover, free molecules of DNA in solution are relatively well-behaved, and therefore afford an excellent experimental system for studies of polymer physics (Smith et al., 1992; Perkins et al., 1994a,b, 1995; Smith et al., 1996; Cluzel et al., 1996). Our own interest in the micromechanical properties of DNA was sparked by recent work monitoring transcription of DNA directed by single molecules of RNA polymerase in vitro (Schafer et al., 1991; Yin et al., 1994, 1995). For such assays, the series elastic compliance of individual DNA molecules must be ascertained and factored into computations of polymerase translocation. We were therefore motivated to develop an improved means of rapidly determining this linkage compliance using the optical trapping system itself, for molecules with lengths around ~1 μm—more than an order of magnitude shorter than sizes used in earlier single-molecule studies of DNA elasticity. In certain respects, our completed instrument resembles feedback-enhanced optical traps recently developed for work with the actomyosin system (Simmons et al., 1996; Molloy et al., 1995), except that the feedback mechanism is implemented by modulating the light intensity instead of the position of the trapping beam. This results in a simpler system with a distinct set of advantages and disadvantages, discussed later. The optical layout for the instrument is shown in Fig. 1 *A*.

The extensibility of DNA has been measured using forces applied by magnets or fluid flow (Smith et al., 1992), and more recently with optical traps (Smith et al., 1996) or glass microneedles (Cluzel et al., 1996). To an excellent approximation, single molecules of DNA behave like ideal, entropic springs for low-to-moderate extension beyond their rest length. The elastic behavior of such springs is characterized by a polymer persistence length, L_P. Data fits to the low-force regime of the *F-x* curve gave persistence lengths of ~53 nm (in 10 mM Na^+ buffer; Bustamante et al., 1994) or ~15 nm (in 80 mM Na^+ buffer, Cluzel et al., 1996). Comparisons of experimental measurements with the predictions of entropic theory have been limited mainly to the low-force regime, where the theory is most applicable. Once drawn out to their full contour lengths, purely entropic springs become inextensible. Molecules of DNA, however, display additional compliance in this limit (Smith et al., 1996), the origin of which is enthalpic and can be characterized by an elastic modulus, K_o. Recently, elasticity theories have been extended to account for both entropic and enthalpic contributions to stretch (Marko and Siggia, 1996; Odijk, 1995). The revised expressions permit a fairly complete comparison with experimental measurements over the full range of extensions, and make possible the simulta-

Received for publication 7 October 1996 and in final form 6 December 1996.

Address reprint requests to Dr. Steven M. Block, 316 Schultz Lab, Department of Molecular Biology, Princeton University, Princeton, NJ 08544. Tel.: 609-258-2638; Fax: 609-258-1035; E-mail: block@watson.princeton.edu.

Dr. Yin's present address is Department of Molecular and Cellular Biology, Harvard University, Cambridge, MA 02138.

0006-3495/97/03/1335/12 $2.00

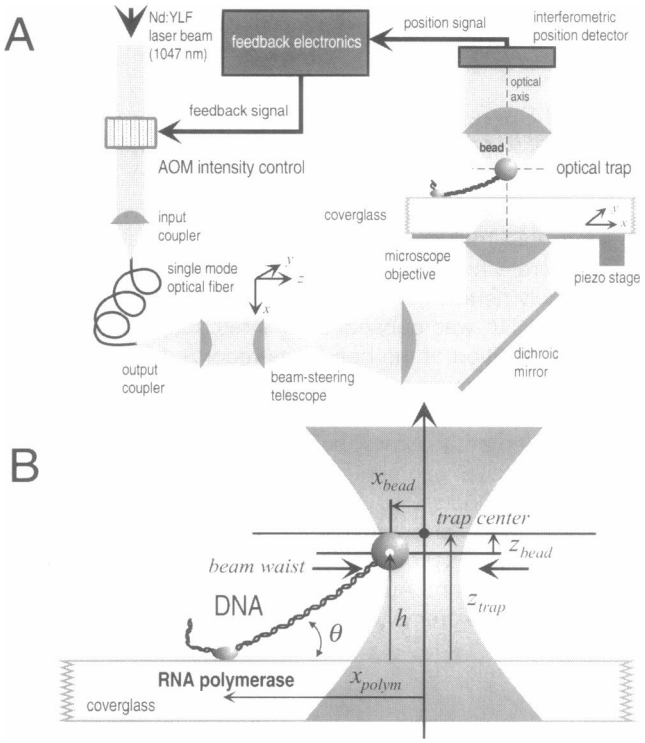

FIGURE 1 (*A*) Simplified optical layout for the feedback-enhanced optical trapping interferometer (not to scale). Laser light passes though an acoustooptic modulator (AOM), which controls the intensity and enters a single-mode, polarization-preserving optical fiber. Light from the output coupler of this fiber is sent to the rear lens of a beam-steering telescope, which is mounted on a three-axis translation stage. Movements of this lens produce *x*-*y*-*z* movements of the optical trap (the telescope also functions as a 2× beam expander). The *z*-axis is always taken to be the direction of the optical axis. Light from the telescope enters the epiillumination path of an inverted microscope and is focused by the objective, forming an optical trap inside the specimen. After passing through the specimen, the laser light is collected in the microscope condenser and passed to an interferometric position detector sensitive to the bead displacement. The position signal from this detector serves as the input to a feedback circuit, which provides a command voltage to the AOM driver. (*B*) Experimental geometry. One end of the DNA is anchored to the coverglass by a stalled RNA polymerase complex. The other end is attached to a bead held in the optical trap, making an angle θ with the coverglass. Forces on the bead cause it to be displaced from equilibrium: note that the bead position (*white dot*) does not coincide, in general, with the position of the trap center (*black dot*) or the laser beam waist (*horizontal arrows*). Various distances, defined in the text, are indicated.

neous extraction of both the persistence length and the elastic modulus.

The current system was developed as a modification to an existing optical trapping interferometer, the features of which have been described previously (Svoboda et al., 1993; Svoboda and Block, 1994a,b). A new feedback clamping feature facilitates measurement by optimizing both weak and strong stretching of DNA in a single measurement. Below the clamp set point, the system operates in open-loop mode, and force develops slowly in proportion to bead displacement. Once the clamp set point is reached, the feedback loop is closed and force develops rapidly without concomitant displacement. By adjusting the clamp point to be in the transition region between low- and high-force regimes, the *F*-*x* relation can be probed with considerable accuracy, even for lengths of DNA as short as ~2 kb (<1 μm). Measurements of extension in such fragments necessitate nanometer-scale resolution of position. In this report we describe the design and operation of our apparatus, particularly aspects of its calibration for both displacement (at the nanometer level) and force (at the piconewton level). We then report data from single DNA molecules subjected to stretch. The elastic properties of these DNA molecules under a variety of ionic conditions are extracted by curve fits to recent theories for polymer stiffness, and the fit parameters are compared with values from other work.

MATERIALS AND METHODS

Optics

To modulate the trapping light intensity, an acoustooptic modulator (AOM) (model 3110-125; Crystal Technology) was inserted between the laser (1047 nm, Nd:YLF; Spectra-Physics TFR) and the input coupler of a single-mode, polarization-preserving optical fiber (Oz Optics). First-order diffracted light from the AOM was introduced into this fiber, which supplies trapping light to an inverted microscope (Axiovert 35; Zeiss). The AOM serves not only to modulate intensity, but also to isolate the laser source (through the frequency shift induced by the acoustic waves), eliminating a previous requirement for an optical isolator, which was removed. In this system the same laser beam is used to trap a particle and to detect its displacement interferometrically. For details of this system minus the feedback enhancement, see Svoboda et al. (1993) and Svoboda and Block (1994a,b). The voltage output from the position-sensing electronics provides input to a custom-built feedback circuit. This circuit generates a command voltage for the AOM controller, modulating the laser intensity as required (and thereby the trap stiffness) to produce an isometric clamp.

Electronic circuitry

The feedback circuit incorporates controls for the position clamp set point, the minimum intensity level, and a variable single-pole, low-pass filter (1–100 kHz). The set-point control determines the displacement at which the feedback loop is automatically closed. The level control sets a minimum below which the laser power may not drop during modulation (required to keep objects stably trapped). The low-pass filter is adjusted to prevent high-frequency oscillations in the feedback loop. These oscillation frequencies are determined by the characteristic times of various components in the loop, including the bead damping time (milliseconds to microseconds), the photodetector preamplifier response time (10 μs), the normalized differential amplifier response time (2 μs), and the AOM itself (0.2 μs). Feedback bandwidth is normally limited by the responses of beads to trapping and/or external forces.

Experimental assay

Chemicals were purchased from various sources, as described previously (Yin et al., 1994). Spermidine was purchased from Sigma. The experimental geometry is essentially identical to that described in our studies of transcription by RNA polymerase (Yin et al., 1995). One end of a DNA molecule is bound to a stalled RNA polymerase complex that is nonspecifically attached to a microscope coverglass surface. The other end is linked to a polystyrene bead (520 nm ± 10 nm diameter; Polysciences) through a biotin-avidin linkage. The experimental geometry is depicted in Fig. 1 *B*. In contrast with earlier experiments, nucleoside triphosphates

(NTPs) are not present in these buffers, so transcriptional elongation does not occur; the enzyme complex merely serves as a convenient way to fix one end of the DNA molecule to the coverglass. During a stretching experiment, the bead is held inside the trap while the stage is moved back and forth with a periodic waveform voltage applied to a piezoelectric stage. As the polymerase is moved away from the trap position, the DNA tether is stretched, pulling the bead from the center of the trap and increasing the restoring force. Once the bead position reaches the clamp set point, feedback is activated, increasing the laser intensity to hold bead position constant while the DNA tether continues to stretch.

The relationship between stage displacement and piezo control voltage was established by tracking beads immobilized on a coverglass surface, using a video-based, centroid cross-correlation method accurate to the subpixel level (Gelles et al., 1988). Distance was established using a diamond-ruled grid with 10 μm spacing, traceable to the National Bureau of Standards (Svoboda et al., 1993).

CALIBRATION METHODS

Trap position control

The trap center is defined as the equilibrium position of the center of an optically trapped sphere with no external load (Fig. 1 *B*). Because of scattering forces, this point does not coincide with the laser beam waist (focus) and will generally be located in a plane beyond the waist, at a distance that depends upon the size of the sphere and its relative refractive index. The trap height, z_{trap}, is defined as the vertical distance between the trap center and the surface of the coverglass, and is affected by the microscope focus. Accurate control of this height is essential to position and stiffness calibration, as well as to establishing a reproducible experimental geometry in DNA stretching experiments. In our system (and all other optical traps), adjusting the microscope's focal control moves both the position of the specimen plane (the position where objects are in focus) and the position of the laser focal plane (hence the trap center). The distance between the trap center and specimen plane can be controlled independently by means of the z-control of an external telescope, which adjusts the convergence of the laser light without alterations to the microscope focus (Svoboda and Block, 1994b; see also Fig. 1 *A*). Trap height was therefore established in two steps. First, an offset between the trap center and the specimen plane was fixed using the external z-control. Next, the trap height was adjusted by refocusing the microscope objective by a preset amount.

Trap center determination

To fix the location of the trap center relative to the specimen plane, the microscope objective was focused directly on the surface of a clean coverglass, as observed by video-enhanced differential interference contrast (VE-DIC) microscopy. Then a freely diffusing bead in buffer was captured and moved vertically toward the surface of the coverglass by using the external z-control only, while the power spectrum of the position signal was continuously monitored. The power spectrum for Brownian motion in a harmonic potential is Lorentzian, with a corner frequency $f_c = \kappa_x/2\pi\beta$, where κ_x is the trap stiffness in the x direction and β is the viscous drag coefficient. Very near the coverglass, this frequency becomes exceedingly sensitive to the proximity of the surface to the bead, because of the strong dependence of drag on height, h (Faxen's law; see Svoboda and Block, 1994b). For example, drag doubles at $h/r \approx 1.2$, where r is the bead radius: the bead is therefore about a radius away from the surface when the corner frequency drops by a factor of ~2. This method was used to set the trap center to one radius over the specimen plane, with an accuracy of $\pm$50 nm for a 0.52-μm-diameter bead.

Trap height determination

Once the distance between trap center and the objective focus was established, the trap height was preset by refocusing the objective a small distance above the coverglass surface. A long indicator arm (~30 cm) was constructed and attached to the fine-focus knob of the microscope; this permitted us to turn the control through a small, reproducible angle, with a focal accuracy of better than 80 nm. Because of the refractive index mismatch at the sample-coverglass interface, the change in focal height is less than the physical movement of the objective lens, by a factor of ~1.2 (Wiersma and Visser, 1996; Hell et al., 1993); this effect was included in estimating the trap height.

Position detector and trap stiffness calibration

The interferometer provides an analog voltage output, V_d, from a normalized differential amplifier encoding displacement. This output is most sensitive to motion along the shear direction of the Wollaston prism in the specimen plane (x direction) and is relatively insensitive to displacements in the y and z directions (unpublished data; Denk and Webb, 1990; Svoboda and Block, 1994a,b). For small displacements, V_d is linear in x_{bead}, hence $x_{bead} = V_d/s$, where s is the sensitivity of the interferometer. Earlier determinations of x_{bead} as a function of V_d had been conducted with silica beads stuck to the coverglass surface and the trap height adjusted to its position of maximum sensitivity, using calibrated stage movements (unpublished data; Svoboda and Block, 1994a).

Three complementary methods of trap stiffness calibration have been described (Svoboda and Block, 1994b):

1. Power spectral estimation. This involves determining the corner frequency of the Brownian motion of the bead, f_c, which depends only on the ratio of the stiffness to the viscous damping.

2. Equipartition theorem. The stiffness is obtained directly from $\frac{1}{2}\kappa_x\langle x^2_{bead}\rangle = \frac{1}{2}k_BT$, where k_BT is Boltzmann's constant times the absolute temperature. This involves measurement of the mean-square displacement of the thermal motion of a trapped bead, $\langle x^2_{bead}\rangle$, using a position-calibrated detector with sufficiently high bandwidth and low noise.

3. Periodic (e.g., sine wave or triangle wave) oscillation. This uses viscous drag forces on a trapped bead applied by oscillating the fluid periodically. For sinusoidal motion, $\kappa_x = 2\pi\beta f_{fluid}(X_{fluid}/X_{bead})$ when $2\pi\beta f_{fluid}/\kappa_x \ll 1$, where f_{fluid} and X_{fluid} are the frequency and amplitude of the fluid movement, and X_{bead} is the amplitude of bead movement. This method is valid over the linear region of the trap, where the stiffness is independent of displacement; by changing the amplitude or frequency of the oscillation, this range can be determined.

Method 1, unlike methods 2 and 3, does not require absolute calibration of the displacement in terms of the position signal; it is only necessary that these two remain proportional. Methods 1 and 3 require knowledge of the viscous drag coefficient β. When beads are close to the surface, small errors in h lead to large errors in β, and therefore κ_x. Method 1 or 3 is therefore best suited when $h > 2r$.

Calibration at trap height

We noted significant differences between the polystyrene beads used for these experiments and the silica beads used for earlier work (Svoboda and Block, 1993, 1994a), attributable to the high refractive index (hence greater light scattering) of polystyrene ($n \approx 1.6$). Because of the greater offset between the beam waist and trap center for polystyrene, the interferometer sensitivity in the plane of the trap center was lower than its maximum sensitivity, which occurs near the beam waist; for silica beads, in contrast, the sensitivities are comparable. Therefore, both s and κ_x become functions not only of the height, h, but also of any axial displacement from the trap center, z_{bead} (Fig. 1 *B*). Such displacements arise, for example, when external forces draw the bead from its equilibrium position. In contrast, for silica beads, neither s nor κ_x varies significantly with h or z_{bead}. Because of such differences, earlier methods of calibration had to be modified, and we adopted the fairly involved procedure described below. In the notation that follows, $s = s(h, z_{bead})$ and $\kappa_x = \kappa_x(h, z_{bead})$, where the arguments refer to the height and vertical offset from the trap center, respectively.

Calibration of the interferometer sensitivity and trap stiffness for a trapped bead was accomplished as follows. At a height sufficient to accurately determine β ($h > 2r$), the positional power spectrum and variance were determined. The stiffness $\kappa_x(h, 0)$ was computed from the corner frequency, and $s(h, 0)$ was computed from the equipartition theorem. Because actual DNA stretching experiments were conducted at $h < 2r$, where the corner frequency becomes less reliable, s and κ_x were obtained by extrapolation from a series of calibrations done over the range h = (600–1600 nm), using the method just described. Within this range, $s^{-1}(h, 0)$ and $\kappa_x(h, 0)$ were nearly linear in h: $s(h, 0)$ and $\kappa_x(h, 0)$ each decreased by ~15% as h increased.

As an internal check on the above method, a determination of $s(r, 0)$ was carried out with beads stuck to the surface, by translating the sample through calibrated x-displacements using the piezo stage; $s(r, 0)$ obtained this way agreed well with extrapolation to $h = r$ by the former approach. This control also shows that the interferometer response, V_d, remains linear with bead displacement out to ~130 nm in the x direction from the trap center.

As a further control (and consistency check), method 3 was used to determine trap stiffness at $h = 1$ μm. This required prior distance calibration of the interferometer, which was performed using methods described above. The stiffness obtained in this way agreed well with that obtained from the power spectrum alone, confirming that the interferometer sensitivity had been properly established. This control further shows that trap stiffness remains constant out to ~140 nm in the x direction from the trap center.

Calibration below trap height

For the general case where the bead is located at an arbitrary height and at an arbitrary z offset from the trap center, $s = s(h, z_{bead})$. This interferometer sensitivity was computed from $s(h,0)$ by scaling from measurements made at one other calibrated location, according to

$$s(h,z_{bead}) = s(h, 0)\frac{s(r,z_{bead})}{s(r, 0)}.$$

where $s(r, z_{bead})$ is the interferometer sensitivity determined at a height equal to the bead radius, $h = r$, using beads stuck to the surface. The sensitivity was then found through calibrated stage translations at different trap heights. This method assumes that the sensitivity, s, for arbitrary h obeys scaling behavior similar to that established for $h = r$, a reasonable approximation when h and r are the same order of magnitude. In these experiments, $s(r, z_{bead})$ typically differed from $s(r, 0)$ by 7–10% under the conditions of study. The $s(r, z_{bead})$ calibration showed the trap center to be located ~290 nm above the plane of maximum interferometer sensitivity. Assuming that this plane corresponds to the location of the laser beam waist, we conclude that the trap center lies ~290 nm from the beam waist for these beads. Trap stiffness $\kappa_x(h, z_{bead})$ was taken to equal $\kappa_x(h, 0)$. The error in this approximation was estimated to be <6%, based on laser beam profile calculations (Visser and Wiersma, 1992).

Geometry determination

Determination of the F-x relationship requires measurements of both force and extension in the direction of the applied stretch, which lies at a variable angle θ in the x-z plane and changes during the course of an experiment (Fig. 1 *B*). These parameters were derived through their geometrical relationship to the interferometer signals in a series of four steps, as follows:

(1) Determine z_{bead} using:

$$z_{bead} = \frac{z_{trap}}{\left(\frac{\kappa_z}{\kappa_x}\right)\left(\frac{x_{polym} - x_{bead}}{x_{bead}}\right) + 1},$$

where κ_x and κ_z are trap stiffness in the x and z directions, respectively. κ_x/κ_z was taken as 5.9, based on the asymmetry of the light distribution near the focus (Visser and Wiersma, 1992). x_{bead} was derived from the interferometer signal at the trap height, according to $x_{bead} = V_d/s(z_{trap}, 0)$. z_{trap} was set before the stretch, and x_{polym} was measured during the course of an experiment (see Results).

2. Use z_{bead} to obtained a revised estimate of x_{bead}, according to

$$x_{bead} = V_d/s(h, z_{bead}).$$

3. Compute the DNA extension, L_{DNA}, from geometry using

$$L_{DNA} = \frac{z_{trap} - z_{bead}}{\sin\left[\tan^{-1}\left(\frac{z_{trap} - z_{bead}}{x_{polym} - x_{bead}}\right)\right]} - r.$$

4. Compute total force exerted by the bead on the DNA from

$$F = \frac{k_x(z_{trap}, 0)x_{bead}}{\cos\left[\tan^{-1}\left(\frac{z_{trap} - z_{bead}}{x_{polym} - x_{bead}}\right)\right]}.$$

For these experiments it was implicitly assumed that the protein-based linkages through which force was applied to the DNA (i.e., the RNA polymerase complex and the biotin-avidin) contributed insignificantly to the total elasticity. This seems reasonable, because these linkages span a distance estimated at ~15 nm, compared to DNA contour lengths on the order of 1 μm. Moreover, it was essential that the point of connection between the DNA and the polymerase complex not move, or, for that matter, that the DNA not break or discontinuously change its elasticity. Slippage of the complex or elastic failure of the DNA could, in fact, be readily detected with our apparatus, and did occur on occasion; tethers that showed either slippage or failure were excluded from further analysis.

RESULTS

Interferometer and trap stiffness calibrations

Before stretching experiments, preliminary calibrations of the interferometer and optical trap were made using untethered beads trapped in buffer, as well as beads fixed to the coverglass surface, as described in Materials and Methods. Variations from bead to bead were quite small (<3%), attributable to the highly uniform size distribution of the polystyrene spheres. Immediately after a stretching sequence on a single DNA molecule, the tethered bead was forcibly detached from the surface using the optical trap, and a series of extensive calibrations were performed at a preset trap height. These calibrations, in combination with the stretch data, were subsequently used to derive the force-extension relationship for the molecule. Control experiments comparing forcibly detached beads to unbound beads did not show any significant differences (*unpublished data*). The trap stiffness measured in all of the buffers used for this study was ~1.1×10^{-3} pN/nm per mW of laser power at the specimen plane. This laser power was calculated from the external power levels and measured transmittance of the optics, as described previously (Svoboda and Block, 1994a).

Intensity-modulated position clamp

This isometric clamp differs somewhat from those developed for single-molecule studies of actomyosin (Finer et al., 1994; Molloy et al., 1995). All present systems use nanometer-level position sensors in conjunction with a feedback arrangement to keep the location of an optically trapped

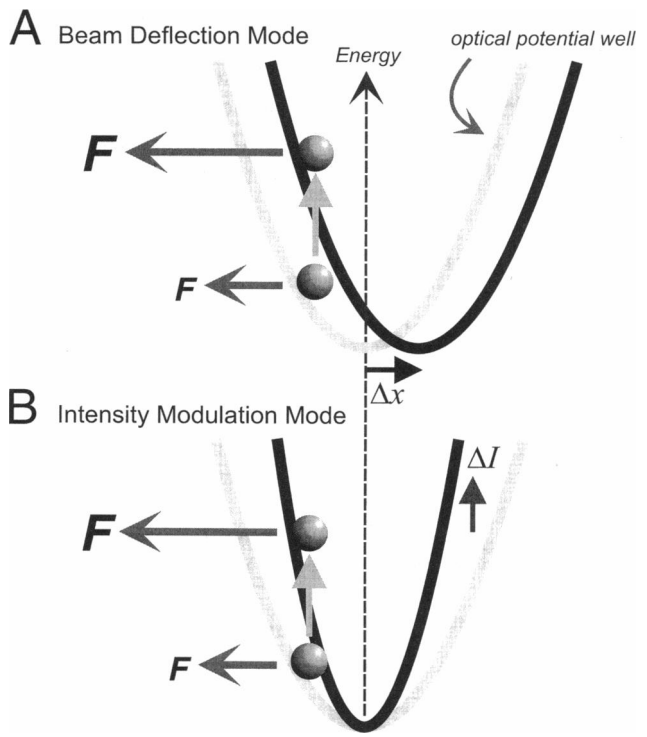

FIGURE 2 Comparison of alternative schemes for establishing a position clamp with an optical trap. Harmonic energy wells are drawn to indicate the optical potentials, such that the vertical height of a bead corresponds to its trapping energy. The force acting on a bead is determined by the slope of the trapping potential at the bead position. Equal and opposite to this is the external force, F, applied to the bead, that the system measures. (*A*) Beam deflection mode (used elsewhere; Simmons et al., 1996; Molloy et al., 1995). The lateral position of the trap is displaced to increase the restoring force on the bead by moving it to a steeper part of the potential. Intensity is not altered; hence trap stiffness stays constant. (*B*) Intensity modulation mode (used here). The light intensity is raised to increase the restoring force on the bead. The position of the trap stays constant, but the stiffness is increased (see text).

object fixed via modulation of the optical restoring force (Fig. 2). In the other devices, the force is altered by deflecting the laser beam in a direction opposite that in which displacement occurs. This effectively stiffens the trap by moving the trapped object into a steeper region of the optical potential (Finer et al., 1994; Simmons et al., 1996). To do so, two orthogonal acoustooptic deflectors (AODs) are used in conjunction with separate position-feedback circuits, one each for x and y deflections. In our system, force is instead changed by modulating the stiffness of the trap, through dynamic adjustments to the light level. This is accomplished with a single AOM that affects trap stiffness in both x and y directions equally. These design differences impart both advantages and drawbacks. First, the system here is optically simpler and more economical to build: AOMs and associated drivers are less costly than AODs, and only a single modulator and feedback circuit are required. Second, this scheme is well suited for use with one-dimensional position sensors (e.g., the interferometer), whereas the other scheme is better suited for use with two-dimensional sensors (e.g., quadrant photodiode detectors). Third, with the intensity-modulated clamp, the light level remains low until it is necessary to increase it; this minimizes local heating, unwanted trapping of free debris, and photodamage to the sample. Finally, our system imposes certain limitations. For example, the clamp position cannot readily be set to the center of the trap—because the restoring force there is zero, independent of stiffness—and therefore the clamp functions best at some finite tension. (However, beam-deflection systems are rarely used to clamp near the origin either, because pretensioning is usually desired to reduce thermal noise.) Moreover, the clamp is unidirectional, in the sense that the restoring force always points toward the center of the trap. In practice, these limitations have not proved troublesome for this work.

Fig. 3 illustrates the operation of the isometric clamp. Here a captured bead was subjected to a periodic square wave of drag force, produced by oscillating the piezo stage with a periodic triangle wave of displacement. With feedback inactive (*left*), the bead was deflected in opposite directions symmetrically. With active feedback (*right*), bead movement continued up to the clamp set point, after which the bead position was fixed. When the bead position was reduced below the clamp set point, the system returned to open-loop mode. Forces computed from the trap stiffness in

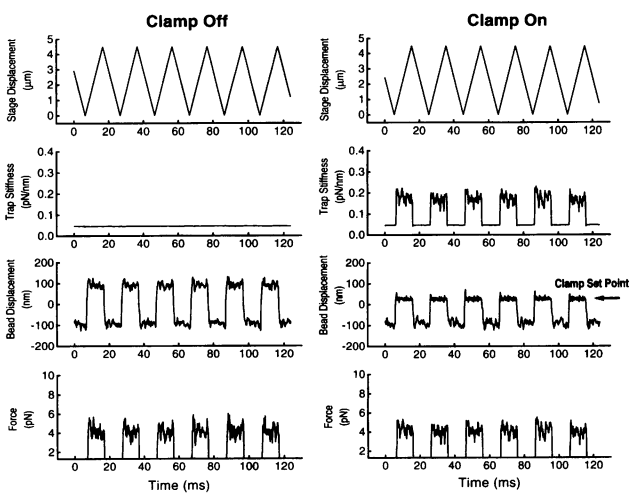

FIGURE 3 Performance of the intensity-modulated position clamp. Panels show the behavior of the system with the feedback system either off (*left*) or on (*right*). In both cases, a freely diffusing bead was first captured by the trap and then subjected to a periodic square wave of drag force, accomplished by moving the stage and specimen with a periodic triangle wave of displacement (*top row*). The trap stiffness remains either constant, or is modulated as required (*second row*). Bead displacement follows a symmetrical square wave with feedback off, but the maximum excursion is clipped to the level of the clamp set point (25 nm) when the system is active (*third row*). Note the increased positional stability (reduction in displacement noise) when the bead clamped. The measured force produced by the stage movement is, within error, identical for both the clamped and unclamped situations, as expected (*bottom row*).

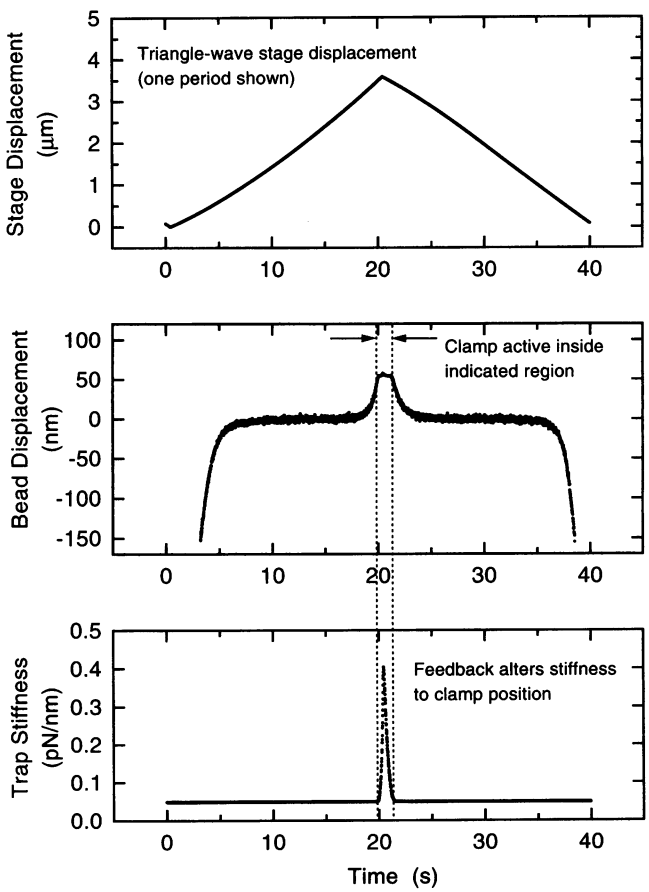

FIGURE 4 Stretching a 3888-bp DNA molecule. (*Top*) The measured stage displacement in response to one period of a triangle wave voltage applied to the piezo stage. Small amounts of curvature, reflecting hysteresis and nonlinearity, are evident in the piezo output (these effects are incorporated in the analysis). (*Middle*) The displacement record of a bead tethered to the coverglass by a DNA molecule subjected to stretch. The feedback clamp is activated for stretching beyond about 60 nm. (*Bottom*) The trap stiffness during the stretch. Note that it remains constant outside of the feedback region, but rises sharply to clamp bead position inside this region.

closed-loop mode were comparable to forces computed from bead displacement in open-loop mode, as expected.

When used to stretch DNA, the instrument operates in two distinct modes, the combination of which allows optimized measurements of both weak and strong forces during stretch (Fig. 4). In open-loop mode, before the clamp position is reached, the feedback is off and the light intensity remains constant; the restoring force is proportional to the product of a time-varying bead displacement and a fixed trap stiffness. Force develops relatively slowly, which facilitates signal averaging in the noisier, low-force region of extension. In closed-loop mode, the feedback is active and the bead is maintained at a constant position; the restoring force is proportional to the product of a fixed bead displacement and a time-varying trap stiffness. Force develops comparatively quickly, allowing a large dynamic range to be probed in the high-force region of extension.

Force-extension relations

Single DNA molecules were stretched repeatedly by fixing the height of the trap to between 360 and 460 nm and applying a periodic triangle-wave voltage to the piezo stage (40-s period). This drive voltage produced stage displacements of 2500–3500 nm (peak to peak). The clamp position was set to a point located 45–120 nm from the trap center, so that beads remained within the linear range of both the detector and trap throughout the stretch. Three data channels were recorded: position detector output, laser light intensity, and piezo drive voltage. Analog position signals were low-pass filtered at 1 kHz, digitized at 2 kHz, averaged with a 20-point boxcar window, and stored by computer. Position and laser signals were converted to x_{bead} and κ_x, as described in Materials and Methods, using calibration data obtained with the same bead immediately after each stretch-

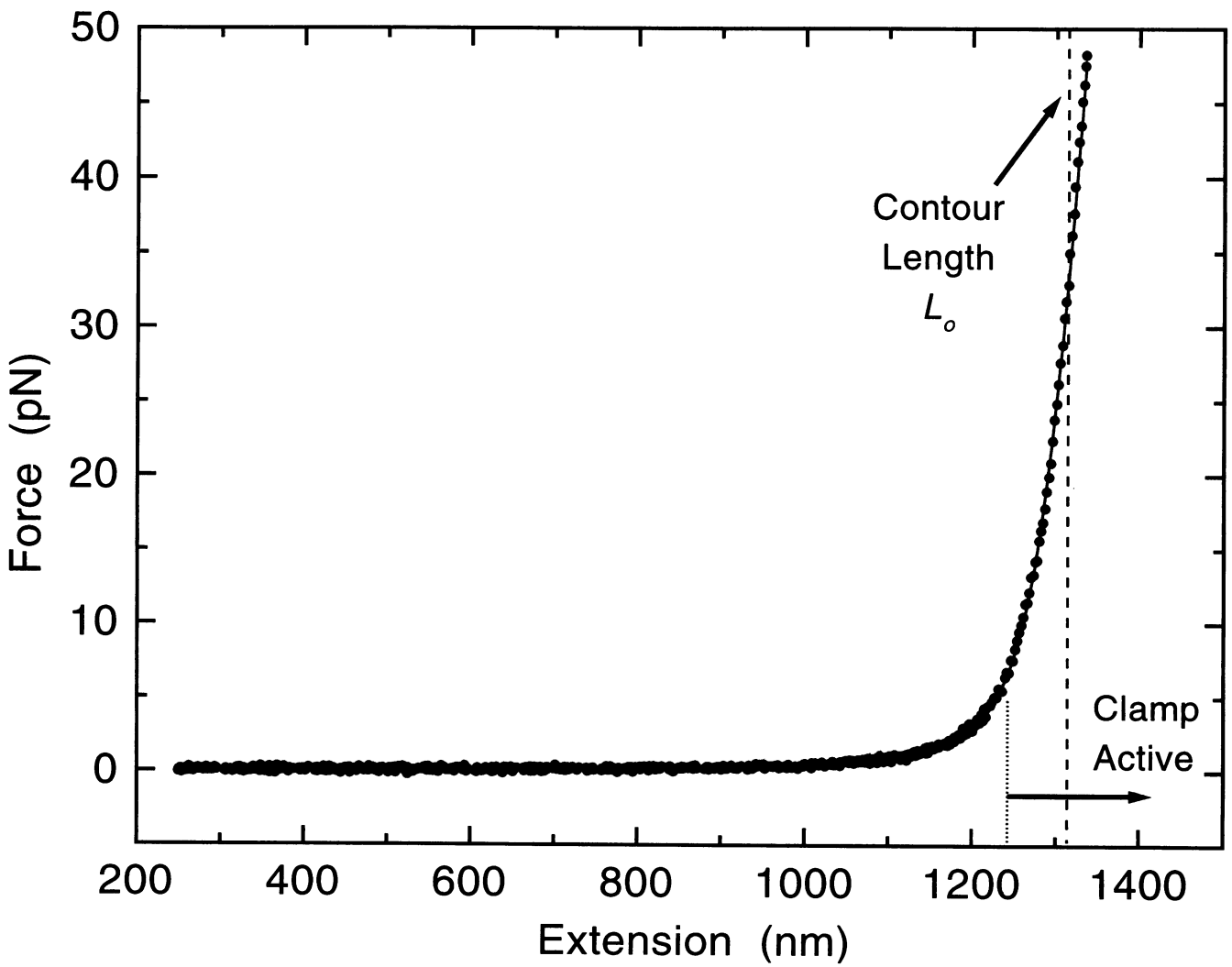

FIGURE 5 The force-extension relationship for a single DNA molecule in PTC buffer (Table 2). Data (*filled circles*) were fit to various models of elasticity, as described in the text. The fit to the modified Marko-Siggia formula (Table 1) is shown (*solid line*). The feedback system was activated beyond a DNA extension of ~1300 nm (*dotted line and arrow*). The contour length of the DNA is ~1314 nm (*dashed line*). Parameter values and associated errors for this fit: L_P = 43.3 ± 0.5 nm, K_o = 1246 ± 10 pN, L_o = 1314 ± 1 nm, p = 0.18. Parameter values and associated errors for fits to other models: Odijk: L_P = 41.2 ± 0.9 nm, K_o = 1296 ± 34 pN, L_o = 1316 ± 1 nm, p = 0.89; Marko-Siggia: L_P = 43.5 ± 1.0 nm, L_o = 1317 ± 2 nm, p = 0.12; FJC: L_P = 3.94 ± 0.03 nm, K_o = 374 ± 2 pN, L_o = 1209 ± 1 nm, $p \approx 0.00$.

TABLE 1 DNA elasticity models

Model	Formula	Comments
Marko-Siggia (1995) WLC	$F = \left(\frac{k_BT}{L_p}\right)\left[\frac{1}{4(1 - x/L_o)^2} - \frac{1}{4} + \frac{x}{L_o}\right]$	Entropic theory. Interpolation formula of exact solution when [salt] ≥ 10 mM. Applicable when $F \ll$ ¼ $(k_BTK_o^2/L_P)^{1/3}$. Differs from exact solution by up to ~10% near $F \approx 0.1$ pN. Approaches exact solution at lower and higher forces.
Odijk (1995) WLC	$x = L_o\left[1 - \frac{1}{2}\left(\frac{k_BT}{FL_P}\right)^{1/2} + \frac{F}{K}\right]$	Entropic/enthalpic theory. Applicable for $\lvert x - L_o\rvert/L_o \ll 1$ (high-force regime).
Smith et al. (1995) FJC	$x = L_o\left[\coth\left(\frac{2FL_P}{k_BT}\right) - \frac{k_BT}{2FL_P}\right]\left(1 + \frac{F}{K_o}\right)$	Entropic/enthalpic theory. Applicable to polymers that approximate a FJC. Note that the Kuhn length = $2L_p$, and Langevin function $L(\alpha) = \coth(\alpha) - 1/\alpha$.
Modified Marko-Siggia WLC	$F = \left(\frac{k_BT}{L_P}\right)\left[\frac{1}{4(1 - x/L_o + F/K_o)^2} - \frac{1}{4} + \frac{x}{L_o} - \frac{F}{K_o}\right]$	Entropic/enthalpic theory. Modification of Marko-siggia formula to incorporate enthalpic stretching. Has limitations similar to Marko-Siggia near $F \approx 0.1$ pN.

WLC, Wormlike chain; FJC, freely jointed chain; F, force; x, extension (end-to-end distance); L_P, persistence length; L_o, contour length; K_o, elastic modulus; k_BT, Boltzmann's constant times absolute temperature.

ing experiment. The stage drive voltage was converted to displacement with appropriate corrections for piezo hysteresis.

In general, the coordinate origin for stage displacement is offset from the equilibrium position of the bead (the position centered over the polymerase) by an unknown amount. The latter position serves as the coordinate origin for the extension under load and was recovered by finding the parity point of the function relating stage and bead displacements (see Appendix). These data were then used to compute single-molecule F-x relationships, an example of which is shown in Fig. 5. DNA was typically stretched by ~25 pN, and in some cases, ~50 pN; forces of this magnitude are below those required to convert DNA to its overstretched form, which has recently been shown to develop with forces in excess of 60 pN (Smith et al., 1996; Cluzel et al., 1996).

DNA elasticity theory

In a simplified picture, the elastic stiffness of DNA may be parameterized by its contour length under zero tension, L_o, a persistence length, L_P, and an elastic modulus, K_o. Persistence length measures the tendency of a uniform, flexible polymer to point in the same direction. Entropic compliance results when the length of a polymer is much greater than this persistence length, owing to the numerous configurations that a polymer may adopt. The elastic modulus, in contrast, measures the polymer's intrinsic resistance to longitudinal strain and reflects enthalpic contributions. The two parameters are generally correlated in wormlike polymers: the longer the persistence length, the greater the stretch modulus. Table 1 summarizes theoretical models for which analytical expressions have been derived; these treat the polymer backbone either as a wormlike chain (WLC) or a freely jointed chain (FJC), and incorporate entropic and/or enthalpic contributions. Note that the various expressions have limited ranges of applicability, depending on a variety of underlying theoretical assumptions. To broaden its range of applicability, we modified the Marko-Siggia interpolation formula (Marko and Siggia, 1995) by adding a stretching term appropriate for intrinsic enthalpic contributions, in a way that corresponds closely to the approach adopted by Odijk (1995).

Fits to theory

Fits were performed of the experimental data to all of the expressions shown in Table 1, using a nonlinear least-squares method (Levenberg-Marquardt algorithm; LabView, National Instruments), with the following results:

1. Marko-Siggia (1995): This is a purely entropic formula and is valid for the lower range of forces. Data for $F < 5$ pN were well fit by the theory. The mean probability, p, of exceeding the experimental value of χ^2 obtained for the model was ~0.27. Systematic deviations between data and fits occurred for larger forces.

2. Odijk (1995): This formula represents a combined entropic-enthalpic theory, applicable at large relative extensions. Data for $F > 2$ pN were also well fit ($p \approx 0.19$). Because the enthalpic term only contributes to stiffness beyond ~9 pN, data sets acquired at lower maximum stretching forces ($F_{max} < 15$ pN) were excluded from the analysis. Parameter and χ^2 values obtained using either Marko-Siggia or Odijk expressions were comparable.

3. Modified Marko-Siggia: This variant of the Marko-Siggia formula fit the experimental data quite well over the complete range of applied force ($p \approx 0.13$); an example is shown in Fig. 5. Fits to data sets acquired at high maximum stretching forces ($F_{max} > 20$ pN) produced parameter values similar to those obtained with either the Odijk or un-

TABLE 2 Summary of DNA elastic characteristics

Buffer composition	L_P (nm) mean ± SE (n)	K_o (pN) mean ± SE (n)	L_o (nm) mean ± SE (n)	L_o expected (nm)
10 mM Na^+ ($NaHPO_4$ buffer, pH 7.0)	47.4 ± 1.0 (14)	1008 ± 38 (10)	1343 ± 5 (10)	1328
150 mM Na^+, 5 mM Mg^{2+} ($NaHPO_4$ buffer, pH 7.0)	43.1 ± 1.3 (5)	1205 ± 87 (5)	1348 ± 6 (5)	1328
10 mM Na^+, 100 μM spermidine ($NaHPO_4$ buffer, pH 7.0)	38.7 ± 1.0 (8)	1202 ± 83 (5)	1313 ± 2 (5)	1328
20 mM Tris, 130 mM K^+, 4 mM Mg^{2+} (PTC buffer, pH 8.0)	41.0 ± 0.8 (15)	1277 ± 57 (12)	1352 ± 3 (12)	1328
20 mM Tris, 130 mM K^+, 4 mM Mg^{2+} (PTC buffer, pH 8.0)	42.1 ± 2.4 (4)	1010 ± 99 (5)	674 ± 5 (5)	661

L_P values were derived from fits to the Marko-Siggia formula for $0 < F < 5$ pN; K_o and L_o values were derived from fits to the Odijk formula for $2 < F < \sim$25–50 pN. Parameter values returned by either method produced almost identical values for L_P and L_o. The expected value for L_o was computed from the number of base pairs in the DNA tether, assuming 0.338 nm/bp (Saenger, 1988), plus an allowance of ~15 nm to account for linkages at either end of the DNA tether. Na-phosphate buffers also contained 0.1 mM EDTA. PTC buffer (not all ingredients listed) was used in the assays of Yin et al. (1995).

modified Marko-Siggia expressions. Fits to partial data sets that excluded the high-force region ($F < 20$ pN) produced some instability in the parameter values. As successively greater portions of the high-force regime were dropped from the analysis, L_P increased, whereas both K_o and L_o decreased. It seems likely that this instability develops from the large difference in stiffness between low- and high-force regions, and the fact that K_o is mainly determined by elastic behavior at the very limit of extension.

4. FJC theory: Experimental data were not well fit by this expression over any force region ($p \leq 10^{-6}$), a finding that supports conclusions of previous work with double-stranded DNA molecules (Smith et al., 1992; Bustamante et al., 1994). The FJC model has, however, been recently applied with some success to the elasticity of single-stranded DNA (Smith et al., 1996).

Effect of ionic strength on DNA stiffness

DNA is a negatively charged polyelectrolyte. Its relatively long persistence length (~50 nm) compared with base pair spacing (0.34 nm) may be partly attributable to mutual electrostatic repulsion of charges along the backbone. Electrostatic screening of such charges is therefore expected to reduce the persistence length. According to polyelectrolyte theory, buffers with sufficient concentrations of mono-, di-, and trivalent ions should neutralize 76%, 88%, and 92% of charges along DNA, respectively (Manning, 1978). Higher valence ions, which are more effective in screening charge, are expected to reduce the persistence length of DNA to a distance near its "intrinsic" value. To study this effect, we combined the expressions in Table 1 with our experimental data to extract the persistence length and elastic modulus for single DNA molecules in buffers containing Na^+, K^+, Mg^{2+}, and spermidine^{3+}.

Spermidine, a trivalent polyamine cation present in a variety of organisms, is thought to facilitate DNA packing by directly screening electrostatic forces. In vitro, spermidine binds DNA and induces condensation (Arscott et al., 1990; Rau and Parsegian, 1992). Our setup permits direct visualization of such condensation: when exposed to solutions containing increasing levels of spermidine (in phosphate buffer, pH 7.0, 10 mM Na^+), the Brownian motion of a variable fraction of DNA-tethered beads was suddenly and dramatically reduced. The remaining fraction of beads continued to diffuse about their tethers. For those tethers that did not condense, we measured the force-extension relationship. These molecules displayed significantly shorter persistence lengths, even in buffers containing 10 mM spermidine, well below the critical concentration for condensation (data not shown).

Table 2 summarizes results of fits in a variety of buffer conditions, including the buffer used for our parallel studies of transcription by RNA polymerase (PTC buffer; Schafer et al., 1991). As a control, measurements were carried out in PTC buffer with two very different sizes of DNA, and the fits returned similar values for L_P and K_o, but dramatically different contour lengths, L_o, as expected. In all cases, fitted contour lengths were in excellent agreement with the computed lengths of tethers, based on the known number of base pairs plus a small allowance for the linkages at either end of the DNA (~15 nm). Persistence length was ~47 nm in a low-sodium buffer (10 mM Na^+), dropped to as low as ~39 nm in buffers containing either Mg^{2+} or 100 μM spermidine^{3+}, but was not further reduced in buffers containing up to 300 μM spermidine^{3+} (data not shown). The elastic modulus, in contrast, appeared to be independent of buffer conditions, at least within the accuracy of these determinations.

DISCUSSION

Persistence lengths computed for 10 mM Na^+ buffers were significantly longer than those in higher salt buffers. The persistence length of DNA did not drop below 39 ± 1 nm, however, even in the presence of multivalent ions expected to neutralize the vast majority of negative charge along the DNA backbone, a result which suggests that the intrinsic persistence length of DNA may be quite close to 40 nm.

Conversely, the elastic modulus was apparently invariant with ionic conditions, although the larger errors associated with determining this parameter may conceal trends in the data. If it is true that the elastic modulus remains nearly constant, then the molecular origin of this parameter may have little to do with charge screening, but may instead reflect interactions intrinsic to the DNA. For an ideal worm-like polymer with uniform, isotropic elastic properties, L_P and K_o are intimately coupled, and both are determined purely by the geometry and Young's modulus. In the simplest possible case, the elastic modulus and persistence length of a solid rod with circular cross section are linearly related through

$$K_o = \left(\frac{16k_BT}{d^2}\right)L_P,$$

where d is the diameter of the rod (Odijk, 1995). Modeling DNA as such a rod (Hogan and Austin, 1987) with $d = 2$ nm (Saenger, 1988) and picking $L_P = 45$ nm (this study) predicts an elastic modulus of ~720 pN, significantly below the value found here and elsewhere (Smith et al., 1996). Choosing instead $d = 1.6$ nm leads to $K_o = 1100$ pN, but the distance seems unreasonably small. In any event, such a simple picture cannot explain the uncorrelated behavior of L_P and K_o. Clearly, both elastic anisotropy and electrostatic interactions must be considered in any comprehensive model of DNA stiffness. For example, a nonuniform cylindrical rod with a radial variation in stiffness, becoming softer away from the central axis, will have a bending stiffness dominated by the relatively weaker compliance contributions at high radii, and this property will be directly reflected in L_P. However, the longitudinal compliance is dominated by contributions that do not depend on the distance from the axis, and will be reflected in K_o. (Put differently, bending stiffness depends on Young's modulus integrated over the cross-sectional moment of inertia, which has an r^4 dependence, whereas the stretch modulus depends on Young's modulus integrated over the cross section, which has an r^2 dependence.) Surface effects, such as electrostatic interactions involving cations, may therefore affect bending more profoundly than stretch. More accurate measurements of DNA elasticity, over an even wider range of ionic conditions, may be required to pin down the relationship between K_o and L_P.

Comparisons with earlier work

Determinations of DNA persistence length in bulk solution have long been carried out using a number of spectroscopic techniques, ranging from light scattering to flow dichroism to electric or magnetic birefringence. Cyclization studies of DNA in solution can also yield values for persistence length, as can electron microscopic measurements on DNA molecules bound to surfaces. All of these approaches are subject to a variety of assumptions; previous characterizations of electrostatic contributions to DNA stiffness have been reviewed and compared (Hagerman, 1988). Some studies find that persistence lengths tend toward an asymptotic limit as the ionic strength of a buffer containing monovalent counterions is increased (Elias and Eden, 1981; Hagerman, 1981; Rizzo and Schellman, 1981; Maret and Weill, 1983; Borochov and Eisenberg, 1984; Porschke, 1991), whereas others report a more or less continuous decrease in persistence length over the experimental range investigated (Harrington, 1978; Kam et al., 1981; Cairney and Harrington, 1982; Sobel and Harpst, 1991). For those groups reporting asymptotic behavior, limiting values of the persistence length range from 44 to 67 nm (with the exception of Borochov and Eisenberg, 1984, who report 28 nm in a solution containing 5 M Li^+), whereas the minimal value found by the other groups ranges from 27 to 38 nm. Studies have generally found that concentrations of divalent counterions in the buffer above 0.1 mM do not significantly reduce persistence lengths below those observed with monovalent counterions above 10 mM (Hagerman, 1988; but see Porschke, 1986). Representative values for persistence lengths in Mg^{2+} solutions include 55 nm (based on transient electric birefringence; Hagerman, 1981), 47 nm (based on DNA cyclization and dimerization; Taylor and Hagerman, 1990), and 44 nm (based on dichroism; Porschke, 1991). The latter value compares closely with numbers in Table 2. The effect of polyvalent ions was reported by two studies that measured linear dichroism, where an asymptotic reduction in persistence length from 79 nm to 45 nm was found after the addition of 10 μM spermidine (Baase et al., 1984), or from 70 nm to 30 nm or 20 nm after the addition of 4 μM spermine or 10 μM cobalt hexamine, respectively (Porschke, 1986). The latter values for persistence length are significantly smaller than our present measurements for spermidine. However, comparisons among bulk methods are problematic because of systematic uncertainties specific to each: light scattering and flow dichroism, for example, rely upon complex data analysis to extract useful numbers, and corrections for hydrodynamics (excluded volume effects, geometry, self-diffusion, etc.) must be applied. Electron microscopic measurements, which involve adsorbing three-dimensional molecules onto a two-dimensional surface, are subject to still further sets of assumptions (Hagerman, 1988; Bednar et al., 1995). Consequently, persistence lengths inferred for similar ionic conditions often differ by factors of 2 from one study to the next. Notwithstanding these difficulties, the present estimate of the intrinsic persistence length (~40 nm) is consistent with earlier work.

In contrast with bulk methods, single-molecule techniques using optical traps and associated nanoscale technologies (Perkins et al., 1994a,b; Smith et al., 1992, 1996; this study) afford an opportunity to make more direct measurements of elasticity, free of many of the assumptions previously required. With the new methods, numbers can be obtained with greater speed, accuracy, and reproducibility. Nevertheless, recourse must then be made to appropriate theories to parameterize elastic behavior in terms of such

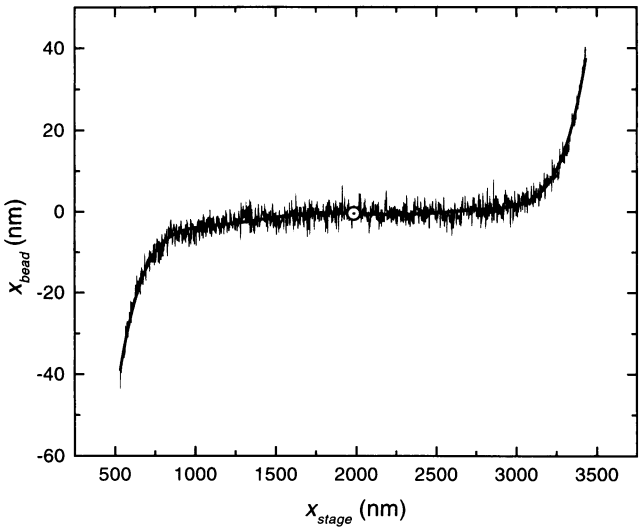

FIGURE 6 Bead position versus stage movement, plotted for the central region of DNA stretch only (unclamped mode), spanning −40 to +40 nm. Raw data (*thin line*) were fit to a seventh-order polynomial (*thick line*). The parity point, located at (x_o = −0.43 nm, y_o = 1985 nm, marked by the *circle*), was determined as described in the Appendix.

quantities as L_P and K_o. The values for L_P reported in Table 2 compare closely with one previous determination under similar ionic conditions by Bustamante and co-workers (53 nm in 10 mM Na^+; Bustamante et al., 1994), but are inconsistent with an approximate value cited by Caron and co-workers, which was a factor of 3–4 smaller (~13–17 nm in 80 mM Na^+; footnote 19 of Cluzel et al., 1996). This discrepancy had been qualitatively ascribed to the increased ionic strength in the latter work, but our determinations at even higher salt concentrations do not support that explanation. It seems more likely that the low figure is attributable to systematic uncertainties in that study, which employed glass microneedles rather than optical traps.

Recently Bustamante and colleagues (Smith et al., 1996) estimated the elastic modulus from their single-molecule data by making a single-point extrapolation based on the high-force behavior of the force-extension curve, reporting a value of 1087 pN (at high ionic strength, in a buffer containing both mono- and divalent ions). This number compares closely to several estimates of the modulus obtained here by direct fits to either the high-force regime alone, using the Odijk formula, or over the complete force range, using the modified Marko-Siggia formula. We anticipate that single-molecule optical techniques similar to those presented here, in conjunction with appropriate theory, will be broadly applicable to the rapid and accurate determination of micromechanical properties for a variety of biopolymers.

APPENDIX

Locating the parity point of an odd function

The parity point of an odd function represents the center of symmetry for that function. We describe here the method used to locate the parity point, (x_0, y_0), of the function $y = f(x)$, where $y = x(t)_{bead}$ and $x = x(t)_{stage}$ from our stretching data, an example of which is plotted in Fig. 6. The procedure can be readily adapted to determine parity points of other odd functions. The experimental data of Fig. 6 were fit with a seventh-order polynomial (this order was chosen empirically: lower-order polynomials did not track the data particularly well, and higher-order polynomials began to track noise). The fit generates eight coefficients (a_0, a_1, . . . , a_7), such that

$$y = f(x) = a_0 + a_1x + \ldots + a_7x^7.$$

Although x_0 is a value close to zero for bead displacement at the center of the trap, there is normally a small offset that we seek to remove by establishing a new origin at the parity point. Because the function is odd about this parity point (x_0, y_0), the fit can be rewritten as

$$y = g(x) = y_0 + b_1(x - x_0) + b_3(x - x_0)^3 + b_5(x - x_0)^5 + b_7(x - x_0)^7,$$

where the new free parameters (x_0, y_0, b_1, . . . , b_7) can be expressed in terms of the fit coefficients (a_0, a_1, . . . , a_7) using the identity

$$\frac{\partial^n f(x)}{\partial x^n} = \frac{\partial^n g(x)}{\partial x^n}$$

for n = (0, . . . ,7). We derive

$$x_0 = -a_6/7a_7 \quad \text{and} \quad y_0 = y(x_0).$$

Alternatively, one could fit to $g(x)$ directly to obtain (x_0, y_0), but this is less convenient, given the availability of standard polynomial fitting routines.

The authors thank these people for their generous help and discussions of the following topics: Eric Siggia, Carlos Bustamante, and Robert Austin for polymer elasticity theory; Koen Visscher and Karel Svoboda for optical theory and design; Lisa Satterwhite for biochemical assays; and Robert Fulbright for data analysis. MDW especially thanks Bart Gibbs and James Ewart for advice on circuit design and construction, and acknowledges the support of the Damon Runyon–Walter Winchell Foundation.

This work was supported by National Institutes of Health grants to SMB, JG, and RL, and a grant from the Whittaker Foundation to JG.

REFERENCES

Arscott, P. G., A.-Z. Li, and V. A. Bloomfield. 1990. Condensation of DNA by trivalent cations. 1. Effects of DNA length and topology on the size and shape of condensed particles. *Biopolymers.* 30:619–630.

Baase, W. A., P. W. Staskus, and S. A. Allison. 1984. Pre-collapse of T7 DNA by spermidine at low ionic strength: a linear dichroism and intrinsic viscosity study. *Biopolymers.* 23:2835–2851.

Bednar, J., P. Furrer, V. Katritch, A. Z. Stasiak, J. Dubochet, and A. Stasiak. 1995. Determination of DNA persistence length by cryo-electron microscopy. Separation of the static and dynamic contributions to the apparent persistence length of DNA. *J. Mol. Biol.* 254:579–594.

Borochov, N., and H. Eisenberg. 1984. Conformation of LiDNA in solutions of LiCl. *Biopolymers.* 23:1757–1769.

Bustamante, C., J. F. Marko, E. D. Siggia, and S. Smith. 1994. Entropic elasticity of λ-phage DNA. *Science.* 265:1599–1600.

Cairney, K. M., and R. E. Harrington. 1982. Flow birefringence of T7 phage DNA: dependence on salt concentration. *Biopolymers.* 21: 923–934.

Cluzel, P., A. Lebrun, C. Heller, R. Lavery, J. L. Viovy, D. Chastenay, D., and F. Caron. 1996. DNA: an extensible molecule. *Science.* 271: 792–794.

Denk, W., and W. W. Webb. 1990. Optical measurement of picometer displacements of transparent microscopic objects. *Appl. Optics.* 29: 2382–2391.

Elias, J., and D. Eden. 1981. Transient electric birefringence study of the persistence length and electrical polarizability of restriction fragments of DNA. *Macromolecules.* 14:410–419.

Finer, J. T., R. M. Simmons, and J. A. Spudich. 1994. Single myosin molecule mechanics: piconewton forces and nanometer steps. *Nature.* 368:112–119.

Gelles, J., Schnapp, B. J., and M. P. Sheetz. 1988. Tracking kinesin-driven movements with nanometer-scale precision. *Nature.* 331:450–453.

Hagerman, P. J. 1981. Investigation of the flexibility of DNA using transient electric birefringence. *Biopolymers.* 20:1503–1535.

Hagerman, P. J. 1988. Flexibility of DNA. *Annu. Rev. Biophys. Chem.* 17:265–286.

Harrington, R. E. 1978. Opticohydrodynamic properties of high-molecular weight DNA. III. The effects of NaCl concentration. *Biopolymers.* 17:919–936.

Hell, S., G. Reiner, C. Cremer, and E. H. K. Steltzer. 1993. Aberrations in confocal fluorescence microscopy induced by mismatches in refractive index. *J. Microsc.* 169:391–405.

Hogan, M. E., and R. H. Austin. 1987. Importance of DNA stiffness in protein-DNA binding specificity. *Nature.* 329:263–266.

Kam, Z., N. Borochov, and H. Eisenberg. 1981. Dependence of laser light scattering of DNA on NaCl concentration. *Biopolymers.* 20:2671–2690.

Manning, G. S. 1978. The molecular theory of polyelectrolyte solutions with applications to the electrostatic properties of polynucleotides. *Q. Rev. Biophys.* 2:179–246.

Maret, G., and G. Weill. 1983. Magnetic birefringence study of the electrostatic and intrinsic persistence length of DNA. *Biopolymers.* 22: 2727–2744.

Marko, J. F., and E. D. Siggia. 1995. Stretching DNA. *Macromolecules.* 28:8759–8770.

Molloy, J., J. E. Burns, J. Kendrick-Jones, R. T. Tregear, and D. C. White. 1995. Movement and force produced by a single myosin head. *Nature.* 378:209–212.

Odijk, T. 1995. Stiff chains and filaments under tension. *Macromolecules.* 28:7016–7018.

Perkins, T. T., D. E. Smith, R. G. Larson, and S. Chu. 1995. Stretching of a single tethered polymer in a uniform flow. *Science.* 268:83–87.

Perkins, T. T., D. E. Smith, and S. Chu. 1994a. Direct observation of tube-like motion of a single polymer chain. *Science.* 264:819–822.

Perkins, T. T., S. R. Quake, D. E. Smith, and S. Chu. 1994b. Relaxation of a single DNA molecule observed by optical microscopy. *Science.* 264: 822–826.

Plum, G. E., P. G. Arscott, and V. A. Bloomfield. 1990. Condensation of DNA by trivalent cations. 2. Effects of cation structure. *Biopolymers.* 30:631–634.

Porschke, D. 1986. Structure and dynamics of double helices in solution modes of DNA bending. *J. Biomol. Struct. Dyn.* 4:373–389.

Porschke, D. 1991. Persistence length and bending dynamics of DNA from electrooptical measurements at high salt concentrations. *Biophys. Chem.* 40:169–179.

Rau, D. C., and V. A. Parsegian. 1992. Direct measurement of the intermolecular forces between counterion-condensed DNA double helices. *Biophys. J.* 61:246–259.

Rizzo, V., and J. Schellman. 1981. Flow dichroism of T7 DNA as a function of salt concentration. *Biopolymers.* 20:2143–2163.

Saenger, W. 1988. Principles of Nucleic Acid Structure. Springer-Verlag, New York.

Schafer, D. A., J. Gelles, M. P. Sheetz, and R. Landick. 1991. Transcription by single molecules of RNA polymerase observed by light microscopy. *Nature.* 352:444–448.

Simmons, R. M., J. T. Finer, S. Chu, and J. A. Spudich. 1996. Quantative measurements of force and displacement using an optical trap. *Biophys. J.* 70:1813–1822.

Smith, S. B., Y. Cui, and C. Bustamante. 1996. Overstretching B-DNA: the elastic response of individual double-stranded and single-stranded DNA molecules. *Science.* 271:795–799.

Smith, S. B., L. Finzi, and C. Bustamante. 1992. Direct mechanical measurements of the elasticity of single DNA molecules by using magnetic beads. *Science.* 258:1122–1126.

Sobel, E. S., and J. A. Harpst. 1991. Effects of Na^+ on the persistence length and excluded volume of T7 bacteriophage DNA. *Biopolymers.* 31:1559–1564.

Svoboda, K., and S. M. Block. 1994a. Force and velocity measured for single kinesin molecules. *Cell.* 77:773–784.

Svoboda, K., and S. M. Block. 1994b. Biological applications of optical forces. *Annu. Rev. Biophys. Biomol. Struct.* 23:247–285.

Svoboda, K, C. F. Schmidt, B. J. Schnapp, and S. M. Block. 1993. Direct observation of kinesin stepping by optical interferometry. *Nature.* 365: 721–727.

Taylor, W. H., and P. J. Hagerman. 1990. Applications of the method of phage T4 DNA ligase-catalyzed ring-closure to the study of DNA structure. II. NaCl-dependence of DNA flexibility and helical repeat. *J. Mol. Biol.* 212:363–376.

Visser, T. D., and S. H. Wiersma. 1992. Diffraction of converging electromagnetic waves. *J. Opt. Soc. Am. A.* 9:2034–2047.

Wiersma, S. H., and T. D. Visser. 1996. Defocusing of a converging electromagnetic wave by a plane dielectric interface. *J. Opt. Soc. Am. A.* 13:320–325.

Yang, Y., T. P. Wescott, S. C. Pedersen, I. Tobias, and W. K. Olson. 1995. Effects of localized bending on DNA supercoiling. *Trends Biochem. Sci.* 20:313–319.

Yin, H., R. Landick, and J. Gelles. 1994. Tethered particle motion method for studying transcription elongation by a single RNA polymerase molecule. *Biophys. J.* 67:2468–2478.

Yin, H., M. D. Wang, K. Svoboda, R. Landick, S. M. Block, and J. Gelles. 1995. Transcription against an applied force. *Science.* 270:1653–1657.